

Optimization of domes against instability

Jihong Ye ^{*1} and Mingfei Lu ²

¹ The State Key Laboratory for GeoMechanics & Deep Underground Engineering,
China University of Mining and Technology, Xuzhou 221116, China

² Key Laboratory of Concrete and Prestressed Concrete Structures of the Ministry of Education,
Southeast University, Nanjing 210018, China

(Received December 25, 2017, Revised May 24, 2018, Accepted June 15, 2018)

Abstract. Static stability is a decisive factor in the design of domes. Stability-related external factors, such as load and supports, are incorporated into structural vulnerability theory by the definition of a relative rate of joint well-formedness (r_r). Hence, the instability mechanism of domes can be revealed. To improve stability, an optimization model against instability, which takes the maximization of the lowest r_r ($r_{r,\min}$) as the objective and the discrete member sections as the variables, is established with constraints on the design requirements and steel consumption. Optimizations are performed on two real-life Kiewitt-6 model domes with a span of 23.4 m and rise of 11.7 m, which are initially constructed for shaking table collapse test. Well-formedness analyses and stability calculation (via arc-length method) of the models throughout the optimization history demonstrate that this proposed method can effectively enhance $r_{r,\min}$ and optimize the static stability of shell-like structures. Additionally, seismic performance of the optimum models subjected to the same earthquake as in the shaking table test is checked. The supplemental simulations prove that the optimum models are superior to the original models under earthquake load as well.

Keywords: domes; optimization; instability mechanism; well-formedness; shaking table collapse test

1. Introduction

Because they are elegant, lightweight and cost-effective, space domes are widely adopted to cover large areas without the use of intermediate supports. As the span increases, static stability rather than strength and stiffness becomes the dominant factor in the design of domes. Therefore, investigation of the instability mechanism and subsequent optimization of the static stability of domes are of theoretical importance and practical value.

The stability of domes was first considered by Kloppel and Schardt (1962). Due to the limitations of computing equipment at that time, the method of continuous shell analogy was used to evaluate the stability. In late 1970s and early 1980s, Riks (1979, 1984) and Crisfield (1983) proposed the arc-length method, a discrete mathematical approach. This approach is described by Ragon *et al.* (2002) as the most effective method for overcoming the divergence problem in the vicinity of limit points and tracing the post-buckling range. In 1990s, Shen and Chen (1999) refined a tangent stiffness matrix for the 3-D column-beam element, thus paving the way for an accurate mathematical model for stability tracing. In the last 30 years, fruitful achievements have been reported in the field of numerical solution, imperfection and post-buckling characteristics (Dubina 1992, Borri and Spinelli 1998, Kashani and Croll 1994,

Papadrakakis 1983). Gioncu (1995) focused on the development and propagation of local instability and summarized all of the instability modes. Liew *et al.* (1997) explored the relationship between member instability and global instability. As for domes of new forms, the stability of various domes, such as hybrid grid shell for barrel vault roof (Cai *et al.* 2013), cable-braced shells (Wang *et al.* 2016, Li and Wu 2017), radially retractable domes (Cai *et al.* 2017a, b), were studied. However, to our knowledge, systematic research on the instability mechanism of space domes is not available in the literature.

To improve the serviceability of domes, size optimization is a topic of investigation (Stolpe 2016, Saka and Geem 2013) and it is a fundamental step in topology optimization (Gholizadeh and Barati 2014, Talaslioglu 2012). Khot (1983) and Levy (1994a, b) optimized pin-joint domes to minimize the weight. In their studies, global stability was in the form of linear eigenvalue problem and was taken as constraints rather than the objective. Linear eigenvalue buckling is not an accurate representation of the stability of domes because it generally overrates the resistance against instability. Moreover, the illustrative examples in the papers are simple pin-joint domes with bar elements. The application of such methods to large-scale real-life domes with beam-column members is doubtful. Pyrz (1990) further considered local stability in the optimization of minimizing the weight. In this study, local stability was in the form of Eulerian buckling stress and global stability was provided by the principle of stationary value of total potential energy. However, the method of the optimization was enumeration which would be inefficient to solve large-scale rigid-joint domes. Saka and Ulker (1992)

*Corresponding author, Professor,
E-mail: jhye@cumt.edu.cn

proposed a method by coupling the nonlinear analysis technique with optimality criteria approach to search out the optimal (lightest) design of pin-joint domes. The difficulty of stability was avoided in the optimality criteria approach because the stability was checked during the nonlinear analysis. The optimization process stopped once the tangent stiffness matrix became singular. Therefore, the result might be near-optimal rather than optimal. Different from all aforementioned methods, Kamat *et al.* (1984) took the stability capacity directly as the objective, rather than constraints, to optimize simple pin-joint models using the principle of stationary potential energy. Talaslioglu (2012, 2013) conducted multi-objective optimization of domes with one of the aims to maximize the load-carrying capacity. In his studies, the buckling critical load traced by the arc-length method was taken as the fitness function in the genetic algorithm. Ghasemi and Hajmohammad (2015) carried out the weight-optimal design of cylindrical shells by genetic algorithm. Parameters of the stiffeners were taken as the optimization variables. However, current optimizations aimed directly at improving the stability fell short of applicability and computational efficiency due to the lack of an instability mechanism.

In 1991, the theory of structural vulnerability was developed according to the connectivity of structural topology (Wu 1991, Lu *et al.* 1999, Agarwal *et al.* 2001). Clustering and unzipping approaches based on joint well-formedness were applied to identify the vulnerable failure scenarios. England *et al.* (2008) applied this theory to risk management of structures, and furthermore Ye *et al.* (2011), Liu and Ye (2014), Nanghai and Jihong (2014) extended the theory to the collapse of space domes and optimized the failure mode.

However, structural vulnerability theory focuses solely on the structure regardless of stability-related external factors, such as load and supports. This paper presents a new vision of structural vulnerability theory with the introduction of the geometric stiffness matrix. External factors are incorporated into classical structural vulnerability theory. This new vision of vulnerability theory is extended to the instability mechanism of domes. To improve the stability, an optimization model against instability is established. Constraints on steel consumption and design requirements are implemented in the optimization, and a modified genetic algorithm is developed especially for this complex problem. Optimizations are performed on two real-life rigid-joint dome models. There are as many as 3660 beam-members in each model. Numerical analyses (traditional arch-length method) are adopted to verify the validity of stability optimization. Finally, the authors check the seismic performances of the optimized domes so that the optimized domes are not inferior to the initial ones (real-life domes). So additional collapse simulations of the optimum domes are performed and the phenomena are compared carefully with the shaking table experiments of the initial domes. This supplemental work shows that the collapse PGA of the optimum models increases dramatically and the collapse mode improves with clear warning signs prior to collapse.

2. Instability mechanism based on joint well-formedness

Structural vulnerability theory builds a hierarchical model of a building by clustering and unzips the model to identify failure scenarios based on joint well-formedness, which has a definite physical meaning (Wu 1991, Lu *et al.* 1999). However, external factors, which exert a tremendous influence on the stability of domes, are not considered in the classical theory.

To consider the external factors (e.g., load and supports), part of the geometric stiffness matrix is introduced to the classical vulnerability theory in this paper. A new vision of structural vulnerability theory characterized by the relative rate of joint well-formedness, which measures joint stability, can reveal the instability mechanism.

2.1 Joint well-formedness in vulnerability theory

Space domes are generally supported at the bottom joints. Different from traditional frames, there are not only vertical force but also horizontal force at the supporting joints. These joints should be supported both vertically and horizontally. At the same time, rotation of these joints is generally constrained to improve the stability of domes. Therefore, the supports of domes are usually fixed supports. By applying the boundary conditions, the completed reduced stiffness matrix \mathbf{K} of a dome composed of n free joints can be expressed as an $n \times n$ partitioned matrix with each block matrix of the same order, i.e.

$$\mathbf{K} = \begin{bmatrix} K_{11} & \cdots & K_{nn} \\ \vdots & \ddots & \vdots \\ K_{n1} & \cdots & K_{nn} \end{bmatrix} \quad (1)$$

where \mathbf{K}_{kk} is the submatrix in \mathbf{K} associated with joint k . The dimension of \mathbf{K}_{kk} , denoted by c , is equal to the number of degrees of freedom of joint k . As for space pinned joint, $c = 3$; as for space rigid joint, $c = 6$. The dimension of \mathbf{K} , denoted by d , is equal to the number of degrees of freedom of the structure.

The equation of a structure can be formulated as

$$\mathbf{F} = \mathbf{K}\mathbf{X} \quad (2)$$

where \mathbf{F} is the global force vector, and \mathbf{X} is the global displacement vector.

According to the properties of the symmetric positive definite matrix, \mathbf{K} can be diagonalized such that

$$\mathbf{K} = \mathbf{P}\mathbf{H}\mathbf{P}^{-1} \quad (3)$$

where \mathbf{P} is an orthogonal matrix, and \mathbf{H} is a diagonal matrix whose elements on the main diagonal are the eigenvalues α_i ($i = 1, 2, \dots, d$) of \mathbf{K} . Note that α_i are all greater than zero.

And we also have

$$\det(K) = \det(PHP^{-1}) = \det(H) = \prod_{i=1}^d \alpha_i \quad (4)$$

Substituting Eq. (3) into Eq. (2) and multiplying the left side of Eq. (2) by P^{-1} leads to

$$P^{-1}F = HP^{-1}X \quad (5)$$

Let

$$\begin{aligned} F' &= P^{-1}F \\ X' &= P^{-1}X \end{aligned} \quad (6)$$

Substituting Eq. (6) into Eq. (5) yields

$$F' = HX' \quad (7)$$

When X' is given a unit vector, that is, $x'_1 = x'_2 = \dots = x'_d = 1$, expand Eq. (7) and it can be presented as follows

$$\begin{aligned} F'_1 &= \alpha_1 \\ F'_2 &= \alpha_2 \\ &\vdots \\ F'_i &= \alpha_i \\ &\vdots \\ F'_d &= \alpha_d \end{aligned} \quad (8)$$

where α_i is defined as the principal stiffness in the direction of the corresponding eigenvector. It can be observed that α_i represents the ability to resist a load along the corresponding axis. And the product of all eigenvalues of \mathbf{K} is equal to the determinant of \mathbf{K} .

As for joint k , its stiffness is provided by all the members which meet at joint k . The stiffness matrix of joint k is the sum of submatrices of \mathbf{k}_{ii} or \mathbf{k}_{jj} of all these members (\mathbf{k}_{ii} applies if i end of the member corresponds to joint k ; \mathbf{k}_{jj} applies if j end of the member corresponds to joint k ; i and j represent two end joints of the member). And it is noticed that the stiffness matrix of joint k equals to \mathbf{K}_{kk} in Eq. (1). According to the physical meaning of the principal stiffness, the well-formedness (Wu *et al.* 1993) of joint k is defined as

$$q_{0,k} = \det(K_{kk}) \quad (9)$$

where $q_{0,k}$ represents the capacity of joint k to resist loads from any direction and is a simple scalar used to measure the global stiffness of a joint. The larger the value of $q_{0,k}$ for joint k , the more robust it is. Additionally, $q_{0,k}$ represents the connectivity of the structure at joint k . The smaller the value of $q_{0,k}$ for joint k , the more vulnerability a structure suffers at this joint.

2.2 Relative rate of joint well-formedness

When a dome is subjected to load, the tangent stiffness matrix is the sum of global stiffness matrix \mathbf{K} and geometric stiffness matrix \mathbf{K}_G . It is known that the geometric stiffness matrix reflects the influence of external factors upon the

overall stiffness. The dome will keep the equilibrium with member forces when it is subjected to external factors (e.g., load and supports). The distribution and amplitude of member forces are closely related to these external factors. And the geometric stiffness matrix of the member is a function of the member force. The global geometric stiffness matrix is the sum of all member geometric stiffness matrix. Therefore, the global geometric stiffness matrix reflects the influence of external factors upon the overall stiffness. The geometric stiffness matrix can be written in such form

$$K_G = \sum k_g^e = \sum k_{gc}^e + \sum k_{gt}^e = K_{GC} + K_{GT} \quad (10)$$

where \mathbf{k}_g is member geometric stiffness matrix; \mathbf{k}_{gc} is the geometric stiffness matrix of a compressive member; \mathbf{k}_{gt} is the geometric stiffness matrix of a tensile member; \mathbf{K}_{GC} is the sum of the geometric stiffness matrix of all compressive members, and \mathbf{K}_{GT} is the sum of geometric stiffness matrix of all tensile members.

The stability of domes depends on not only the structure itself but also external factors (e.g., load and supports) greatly. So, external factors should be introduced into the vulnerability theory when stability is considered. But different from common frames, domes depend heavily on shape to resist loads, as characterized by the membrane effect. Most of the members are in compression. The distribution and magnitude of compressive stress directly determine the stability of the dome. Thus, it is \mathbf{K}_{GC} that takes on the stability-related influence of external factors upon the deterioration in structural stiffness. In this regard, \mathbf{K}_{GC} is introduced to define the joint well-formedness from the aspect of stability

$$q_{1,k} = \det(\mathbf{K}_{kk} + K_{GCkk}) \quad (11)$$

where \mathbf{K}_{kk} is given by Eq. (1), \mathbf{K}_{GCkk} is the submatrix in \mathbf{K}_{GC} associated with joint k , and \mathbf{K}_{GC} is referred in Eq. (10).

By analogy, $q_{1,k}$ indicates the global stiffness of joint k subjected to load. The variation in the well-formedness of joint k after the introduction of \mathbf{K}_{GC} is defined as the absolute rate of well-formedness, denoted as $r_{a,k}$

$$r_{a,k} = q_{1,k} - q_{0,k} \quad (12)$$

where $q_{1,k}$ and $q_{0,k}$ are defined in Eq. (11) and Eq. (9), respectively. $r_{a,k}$ evaluates the stiffness deterioration of joint k in that a low $r_{a,k}$ indicates a remarkable degeneration of joint stiffness and vice versa.

To consider the internal and external factors, the relative rate of well-formedness of joint k is defined as

$$r_{r,k} = r_{a,k}/q_{0,k} \quad (13)$$

where $r_{a,k}$ is the absolute rate of well-formedness of joint k , and $q_{0,k}$ is the well-formedness of joint k .

Compared with $r_{a,k}$, $r_{r,k}$ assesses the deterioration of joint k relative to its own $q_{0,k}$. Therefore, $r_{r,k}$ measures the stability of joint k internally and externally. According to r_r ,

buckling areas even instability joints can be identified, and the instability mechanism can be revealed.

2.3 Instability mechanism

According to the cause and process of the failure of structures, six types were classified by Starossek (2007), i.e., pancake-type, zipper-type, domino-type, section-type, instability-type and mixed-type collapse. From the perspective of the robustness, vulnerability theory can be used to analyze zipper-type collapse. The new vision of the theory proposed in this paper is extended to instability-type collapse. The relative rate of well-formedness quantitatively measures the stiffness degeneration, indicating the tendency toward instability. Hence, the instability mechanism is revealed. Whatever it is pin-joint dome or rigid-joint dome, the instability mechanism is both applicable.

- Compressive elements in the dome lead to the deterioration of relative joints, which therefore have low r_r . According to the value of all joints' r_r , joints with lower r_r have the relatively-remarkable tendency to instability. The dome does not lose stability until these joints or additional joints lose the capacity to resist any further incremental load. Among all the joints, the one that possesses the lowest value (denoted as $r_{r,\min}$ and defined in Eq. (15)) suffers the most deterioration in stiffness and is inclined to lose its stability at first. Rigorously, the total stiffness deterioration of this joint can be a sufficient condition for the loss of stability, but it is not a necessary one.
- Given the same configuration (i.e., span, rise, topology and supports) and subjected to the same load, domes with low $r_{r,\min}$ have a low capacity of stability due to the relatively weak zones, whereas these with high $r_{r,\min}$ have a high capacity for stability due to the well-distributed stiffness.

Different load levels, which are subjected to the same load mode, lead to different \mathbf{K}_{GC} and further the variation of the value of each joint's r_r . But the sequence of joints, which are sorted by r_r in ascending / descending order, does not vary. Therefore, the distribution pattern of all joints' r_r is irrelevant to load level.

3. Optimization against instability based on joint well-formedness

3.1 Optimization objective

According to the instability mechanism, a high value of $r_{r,\min}$ is favorable to the buckling resistance of domes. Thus the optimization model against instability takes the maximum of $r_{r,\min}$ as the optimization objective, denoted as

$$\text{Maximize } r_{r,\min} \quad (14)$$

where $r_{r,\min}$ is defined as

$$r_{r,\min} = \min(r_{r,1}, r_{r,2}, \dots, r_{r,k}, \dots, r_{r,n}) \quad (15)$$

3.2 Optimization variables

Section designations are taken as discrete optimization variables. Member grouping strategy is not adopted here because the stability of space dome is sensitive to the section designation of each member. The section size of each member is represented as an independent variable. Considering engineering applications, the sections available are chosen from Chinese manufacturing standards GB/T 17395-2008 (2008) as discrete variables. The optimization variables can be stated as follows.

Find

$$\mathbf{I} = [I_1, I_2, \dots, I_i, \dots, I_m] \quad (16)$$

to generate

$$\mathbf{S} = [S_1, S_2, \dots, S_i, \dots, S_m]^T \quad (17)$$

$$S_i = [D_i, t_i]$$

where \mathbf{I} is a vector of integer values, representing the sequence numbers of available sections in a section table; \mathbf{S} , generated according to vector \mathbf{I} , is a matrix of section sizes for all the members of the structure; D_i and t_i are the external diameter and thickness of the i th member, respectively; m is the total number of structural members.

3.3 Constraints

The constraint on steel consumption is defined in Eq. (18). As for real-life single-layer domes, joints should be connected rigidly. So all the elements of the dome are beam-column members. Constraints on design requirements of beam-column members are defined in Eqs. (19)-(21) according to Chinese code GB50017-2003 (2003) and specification JGJ7-2010 (2010).

(1) Steel consumption constraint

$$V_i \leq \eta_V \times V_0 \quad (18)$$

where V_i is the steel volume of the optimum dome after the i th iteration, V_0 is the steel consumption of the initial model, and η_V is the steel volume adjustment coefficient.

(2) Slenderness constraint

$$\lambda_i = \frac{l_{0i}}{i} \leq [\lambda] \quad (19)$$

where λ_i is the slenderness ratio of the i th member, l_{0i} is the calculated length of the member, i is the radius of gyration and $[\lambda]$ is the allowable slenderness ratio.

(3) Strength constraint

$$\frac{N_i}{A_{ni}} \pm \frac{M_{xi}}{\gamma_x W_{nxi}} + \frac{M_{yi}}{\gamma_y W_{nyi}} \leq f \quad (i = 1, 2, \dots, n_m) \quad (20)$$

where N_i is the axial force of the i th member, A_{ni} is the net sectional area of the i th member, M_{xi} and M_{yi} are the bending moments along two principal axes, γ_x and γ_y are the admissible plastic coefficients of the cross-section, W_{nxi} and W_{nyi} are the net section modules along the two principal axes, and f is the design strength of the material.

(4) Element stability constraint

$$\frac{N_i}{\varphi_{yi} A_i} + \frac{\beta_{myi} M_{yi}}{\gamma_y W_{yi} \left(1 - \frac{0.8N_i}{N_{Ei}}\right)} + \eta \frac{\beta_{txi} M_{xi}}{\varphi_{bxi} W_{xi}} \leq f \quad (21)$$

$(i = 1, 2, \dots, n_m)$

where A_i is the cross-sectional area of the i th member, φ_{yi} is the stability coefficient of axial compression, β_{myi} and β_{txi} are the equivalent bending moment coefficients in-plane and out-of-plane of the bending moment, respectively, W_{xi} and W_{yi} are the section modules along the two principal axes, η is the sectional influence coefficient, φ_{bxi} is the integral stability coefficient of the member under uniform bending and N_{Ei} represents the Euler critical force.

3.4 Modified genetic algorithm

The genetic algorithm (GA) is a stochastic search algorithm that imitates evolution in the natural environment. The GA was proven by Artar (2016) that it was a powerful meta-heuristic search technique for dome optimization. Considering the deficiency of GA, the random mutation operation in the traditional GA is modified into guided mutation to improve the optimization efficiency. A modified GA consists of the following steps:

- (1) Encoding: A binary encoding scheme suitable for discrete variables is adopted. The sequence number of each section in decimal form is transformed into binary form.
- (2) Fitness calculation: The fitness function is used to evaluate an individual's fitness, which is a formal measure of perceived performance as defined by the environment. The unconstrained function $f(x)$ is constructed as

$$f(x) = \frac{1}{|r_{r,\min}|} \quad (22)$$

where x represents an individual in the population. For the steel volume constraint, a rejection strategy is adopted such that chromosomes that violate Eq. (18) are discarded. For design constraints, a penalty strategy is used to transform the constrained problems into an unconstrained form by penalizing infeasible solutions. The penalty function $p(x)$ proposed by Gen and Cheng (1996) is constructed as follows

$$p(x) = 1 - \frac{1}{m} \sum_{i=1}^{m_v} \frac{\Delta b_i(x)}{\Delta b_i^{\max}} \quad (23)$$

$$\Delta b_i(x) = \max\{0, g_i(x) - b_i(x)\}$$

$$\Delta b_i^{\max} = \max\{0, \Delta b_i(x)\}$$

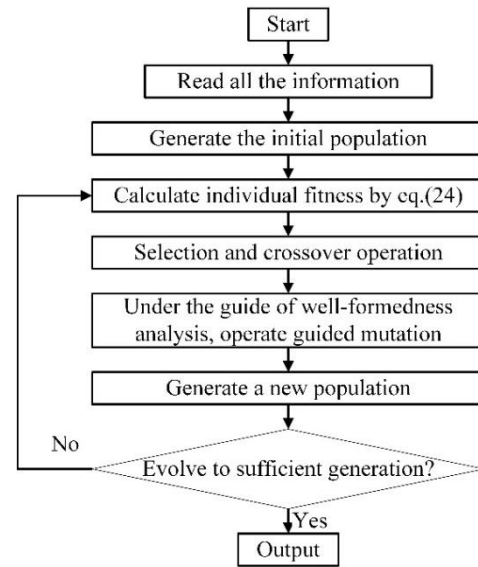


Fig. 1 Modified GA program flow

where $\Delta b_i(x)$ is the value of violation for the i th constraint, $\Delta b_{max i}(x)$ is the maximum of violation for the i th constraint among the current population, m_v is the number of violated constraints and ε is a small positive number used to ensure that the penalty avoids zero division.

With respect to the penalty function, the final fitness function is calculated as

$$F(x) = p(x)f(x) \quad (24)$$

- (3) Selection and crossover operation: The selection operation uses bias towards individuals with better fitness and thus, the selected child has higher fitness. All individuals are sorted in terms of fitness first, and truncation selection is adopted with the best quarter of the population copied twice and the medium half copied once to form a new population. The crossover operation exchanges a subset of the parent genes with a given crossover probability to create two new individuals.
- (4) Guided mutation: Buckling zones are identified according to the well-formedness analysis (section 2), and the corresponding genes are positioned where mutation is operated under the guide of well-formedness analysis.

The flowchart of the modified GA is shown in Fig. 1. Details can be referred in our newest paper (Lu and Ye 2017). The corresponding algorithm is coded on the platform of MATLAB.

4. Optimization of real-life dome models

4.1 Model information

The illustrative examples are two real-life K6 models. Each model (see Fig. 2) was constructed with a span of 23.4 m and rise of 11.7 m. A total of 40 rigid supports (see Fig.

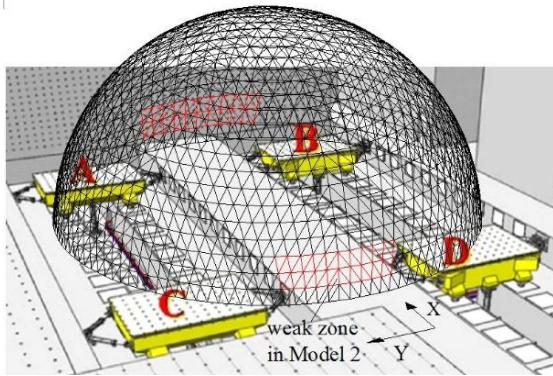


Fig. 2 Model and shaking tables



Fig. 3 Constraints on shaking table

3), which were uniformly distributed on each shaking table, were fixed on the periphery of each model. As many as 1261 welded hollow sphere joints (rigid joints) and 3660 members (beam members) were assembled in each model. Both models had the same steel consumption. Model 1 had a uniform stiffness distribution while Model 2 had a nonuniform stiffness distribution with two weakened zones (red area in Fig. 2) and a stiffened top. Fig. 4 shows the member arrangements of both models. The members of the weak zone in model 2 were $\Phi 18 \times 1$ and those with top reinforcement were $\Phi 38 \times 2$.

These two models were mainly designed for shaking table test. Details of the shaking table tests and dynamic analyses can be referred in our newest paper (Xu and Ye 2017). However, considering the scale, the complexity and the difference of the two models, it is suitable and persuasive to use these models as the validation of the proposed optimization.

The analysis procedure of these two real-life domes are divided into 3 steps. In the first step, optimization of the two domes against instability based on joint well-formedness (section 3) is conducted. In the optimization process, well-formedness analyses (section 2) are performed to investigate the stability of domes and to calculate the fitness function. After optimization, we get all the generated domes throughout the optimization process, including the final optimum one. In the second step, we calculate the buckling load (P_{cr}) of each generated dome via traditional arch-length method. And then the history of P_{cr} throughout the optimization is drawn to confirm whether the stability is elevated by optimization. Finally in the third step, supplemental seismic analysis is conducted on the optimum domes only to check their collapse resistance.

4.2 Optimization subjected to uniform distributed load

The members with specification of $\Phi 114 \times 4$ remain the same because they function as the supporting ring. The sections available are as follows: for sections with outer diameter ranging from 18 mm to 48.3 mm, the corresponding thickness is no more than 2 mm; for sections with outer diameter ranging from 50 mm to 114 mm, the corresponding thickness is no more than 4 mm. There are totally 580 candidate sections which can be referred in Chinese manufacturing standards GB/T 17395-2008 (2008). The dome has 3660 members and the number of design variables is equal to 3660. The initial models satisfy the requirements of similarity and consider the related specifications. Thus, the constraint on the steel volume is slightly relaxed with the expectation that the optimum domes satisfy the design requirements. Therefore, $\eta_V = 1.07$. Unit load level, which represents the load mode, is adopted

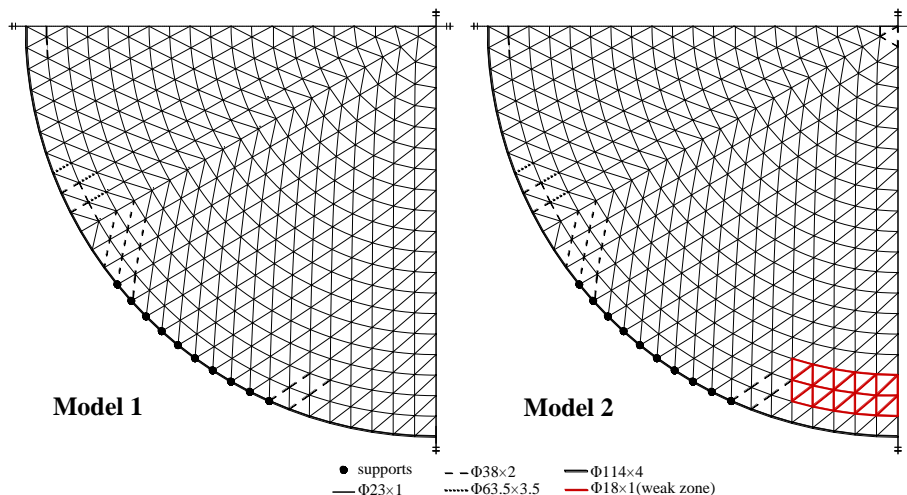


Fig. 4 Structural arrangements

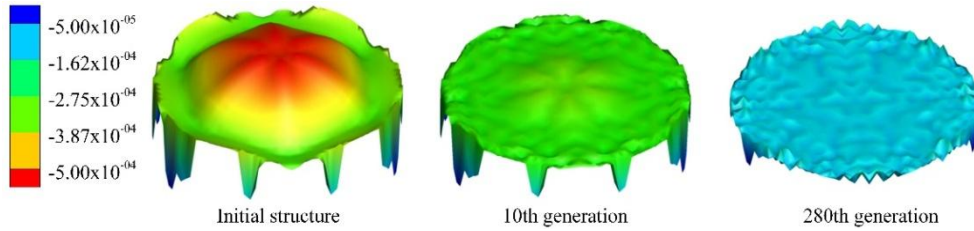


Fig. 5 Distribution of r_r in the process of optimization

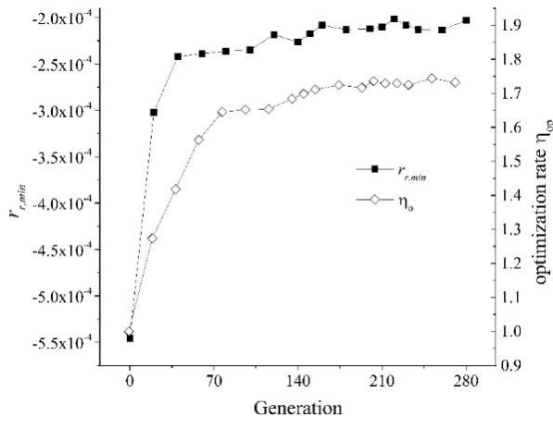


Fig. 6 $r_{r,min}$ and η_o in the optimization process

for the calculation of \mathbf{K}_{GC} in Eq. (10).

The optimization rate (η_o) is introduced to measure the effectiveness of optimization after the i th generation

$$\eta_o^i = P_{cr}^i / P_{cr}^0 \quad (25)$$

where P_{cr}^i is the elastic buckling load for the dome of the i th generation; and P_{cr}^0 is the buckling load for the initial model; both values are gained by arc-length method.

4.2.1 Model 1

For the initial dome, $V_0 = 0.3500 \text{ m}^3$, $r_{r,min} = -5.457 \times 10^{-4}$ and $P_{cr}^0 = 3.27 \text{ kN/m}^2$. The distribution of r_r and variation curves of $r_{r,min}$ and η_o throughout the optimization process are shown in Figs. 5-6, respectively.

Figs. 5-6 show the followings:

- $r_{r,min}$ increases dramatically in the first 70 generations, and the distribution of r_r tends to be uniform at the same time. Accordingly, η_o increases remarkably within this process.

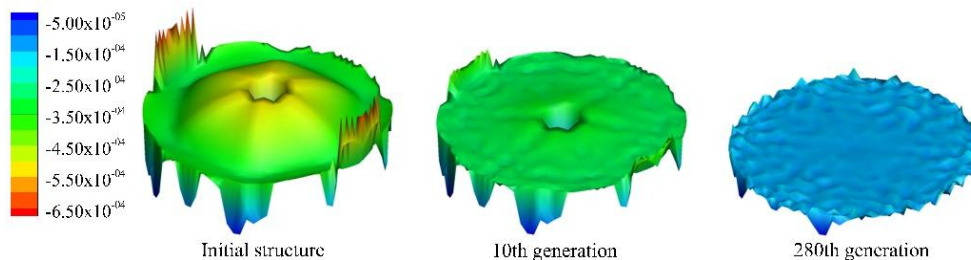


Fig. 8 Distribution of r_r in the process of optimization

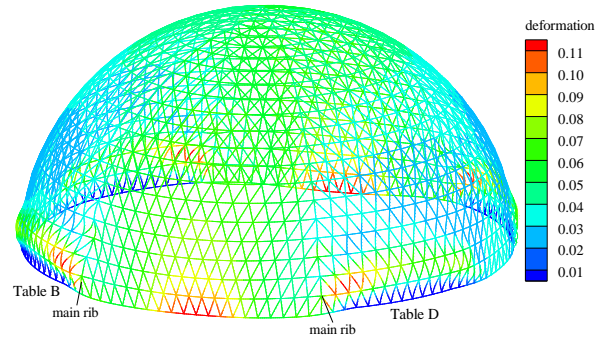


Fig. 7 Buckling mode of optimum dome (unit: m)

- After the population evolves to the 70th generation, $r_{r,min}$ converges to the optimum value and remains stable, whereas η_o increases slightly and remains steady as well within a short time.

For the optimum case: $r_{r,min} = -2.029 \times 10^{-4}$ and r_r distribute uniformly, indicating a reasonable stiffness distribution, and $V = 0.3724 \text{ m}^3 < \eta_V \times V_0$, $P_{280 cr} = 5.666 \text{ kN/m}^2$, and $\eta_{280 o} = 1.732$. It means the buckling capacity of the optimum dome is 1.732 times greater than that of initial model. The buckling mode, with deformation magnified 5 times, is described in Fig. 7. The members directly above the four tables, especially these near the main ribs, deform remarkably.

4.2.2 Model 2

Due to the weakness and reinforcement in model 2, its stiffness distribution is uneven and irregular. The weak zones have low r_r , including $r_{r,min} = -6.991 \times 10^{-4}$, whereas the reinforced zone has high r_r . For the initial dome, $V_0 = 0.3498 \text{ m}^3$ and $P_{cr}^0 = 3.13 \text{ kN/m}^2$. The distribution nephogram of r_r during the optimization process is presented in Fig. 8. The variation curves of $r_{r,min}$ and η_o in the optimization are shown in Fig. 9.

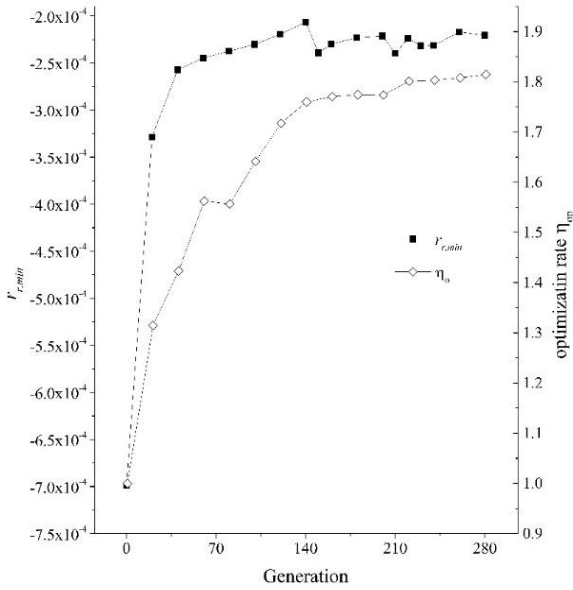


Fig. 9 $r_{r,min}$ and η_o in the optimization process

Figs. 8-9 show the followings:

- At the first stage, $r_{r,min}$ increases, and the distribution of r_r , especially that of the weak zones, tends to be uniform simultaneously. At the same time, η_o increases in a step-by-step manner.
- Both $r_{r,min}$ and η_o converge to optimal value and remain stable after the 210th generation.
- For the optimum dome, $r_{r,min} = -2.204 \times 10^{-4}$. The distribution of r_r is uniform, indicating a reasonable stiffness distribution, and $V = 0.3741 \text{ m}^3 < \eta_V \times V_0$ and $P_{280 cr} = 5.672 \text{ kN/m}^2$, leading to $\eta_{208 o} = 1.812$. It means the buckling capacity of the optimum dome increases 1.812 times.

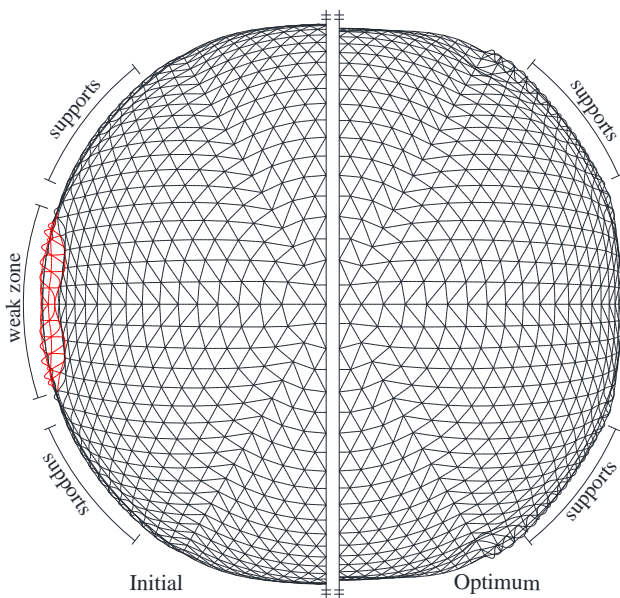


Fig. 10 Buckling modes of initial & optimum domes (plan view)

Table 1 Comparison of optimum results

Parameters	Model 1		Model 2	
	Initial model	Optimum model	Initial model	Optimum model
$r_{r,min}$	-5.457×10^{-4}	-2.029×10^{-4}	-6.991×10^{-4}	-2.204×10^{-4}
P_{cr} (kN/m ²)	3.27	5.666	3.13	5.672
V (m ³)	0.3500	0.3724	0.3498	0.3741

The buckling modes of the initial dome and the optimum dome are obtained by the arc-length method. Due to the symmetry, half of each buckling mode, the deformation of which is magnified 5 times, is demonstrated in Fig. 10. The weak zones in the initial dome with low r_r (see Fig. 8) buckle prior to the remainder of the structure. The initial dome presents local instability in that the two weak zones merely lose stability. However, for the optimum dome, the instability mode is transformed by optimization. No instability occurs in the location that used to buckle as weak zones. The buckling areas are located above four tables, particularly near the main ribs, because of force concentration. The buckling mode of the optimum dome of model 2 shares similarity with that of model 1 (see Fig. 7), which is clarified in the following section (Section 4.2.3).

4.2.3 Comparison of optimum results

The parameters of two optimum domes subjected to uniform load are listed in Table 1. The buckling modes of optimum domes are described in Figs. 7 and 10, respectively. Although the initial models show differences, the two optimum ones have nearly the same steel volume, similar $r_{r,min}$ and nearly equal P_{cr} . In addition, their buckling modes share similarities in that the buckling areas are all located above the supports. The comparison illustrates that given the topology and steel consumption, the optimization reaches the optimum result regardless of the initial structure and retains the best solution despite the continuation of optimization. Hence, the optimization method proves to be effective and robust.

4.3 Check on seismic performances of the optimum domes

The seismic performances of the optimal domes are checked so that the optimized domes are not inferior to the initial domes. The shaking table test of the original models was conducted in Tongji University, China. The seismic wave for numerical simulation is the same as experiment. The simulations of two initial domes correspond well with the experiment (Xu and Ye 2017), which validate the numerical models.

4.3.1 Model 1

4.3.1.1 Description of shaking table test for initial dome

The initial dome vibrated slightly when the peak ground acceleration (PGA) reached 100 gal. As the PGA reached 200 gal, a few members at the bottom between table A and

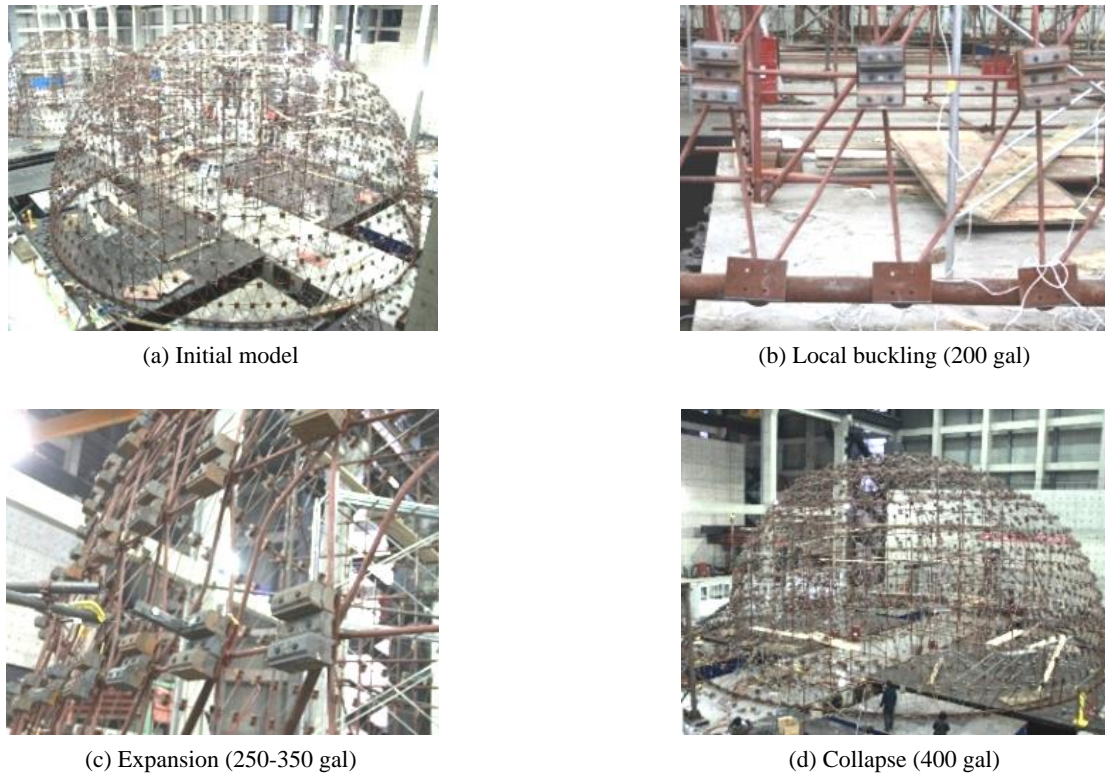


Fig. 11 Experiment of model 1

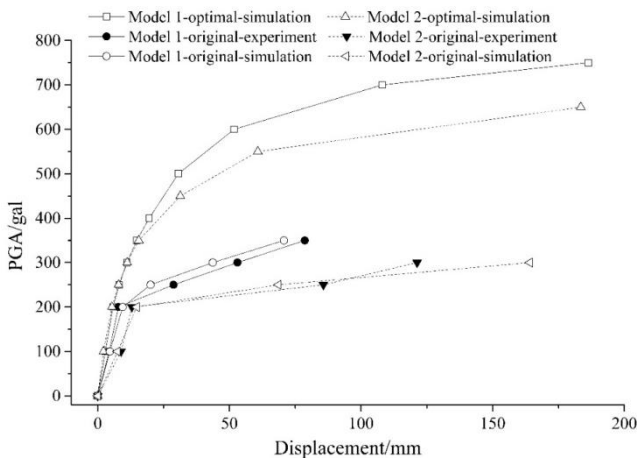


Fig. 12 Load-displacement curve of initial and optimum domes for both models

table D began to bend while the rest remained elastic (Fig. 11(b)). When the PGA increased from 250 gal to 350 gal, certain diagonal members of the second to fifth loops (from the bottom to top) located between table C and table D were bent gradually (Fig. 11(c)). The material in this component entered plasticity. Finally, when the PGA increased to 400 gal, the deformation of the aforementioned zones was augmented quickly with a dramatic depression of related joints, leading to immediate failure (Fig. 11(d)). In this case, the instability mode and collapse mode are possibly connected. When subjected to an earthquake, the model vibrates intensively where the buckling deformation is notable.

The PGA- Δ curve (Fig. 12) is bilinear with a gentler slope after the PGA reaches 200 gal. The initial dome under earthquake action presents a collapse mode with certain signs.

4.3.1.2 Seismic performance of optimum structure

On the LS-DYNA platform, seismic analysis is conducted on the optimum dome listed in Table 1. The elastic modulus and the yield strength adopted in the simulation are chosen in accordance with the initial model.

No obvious deformation of the optimum dome is observed until the PGA reaches 400 gal. When the PGA increases to 500 gal, only the diagonal members of the second to fourth loop, located near the main ribs and above the tables, start to bend. The bending areas extend as the PGA reaches 600 gal. When the PGA increases to 750 gal, the diagonal members in the third loop above table B and table D become convex, whereas the ones in the fifth loop become concave, presenting a wave-shaped deformation. When the PGA increases up to 800 gal, the dome collapses from the aforementioned buckling areas. The load-displacement curves in Fig. 12 show that the collapse PGA for the optimum dome is 800 gal, and the critical value for the initial dome is 400 gal. The collapse PGA of the optimum dome is elevated by a factor of 2. It can also be concluded that the PGA- Δ curve of the optimum dome tends to be gentle as PGA increases, giving clear warnings prior to collapse.

4.3.2 Model 2

4.3.2.1 Description of shaking table test for initial structure

When the PGA was 100 gal, the dome oscillated gently.

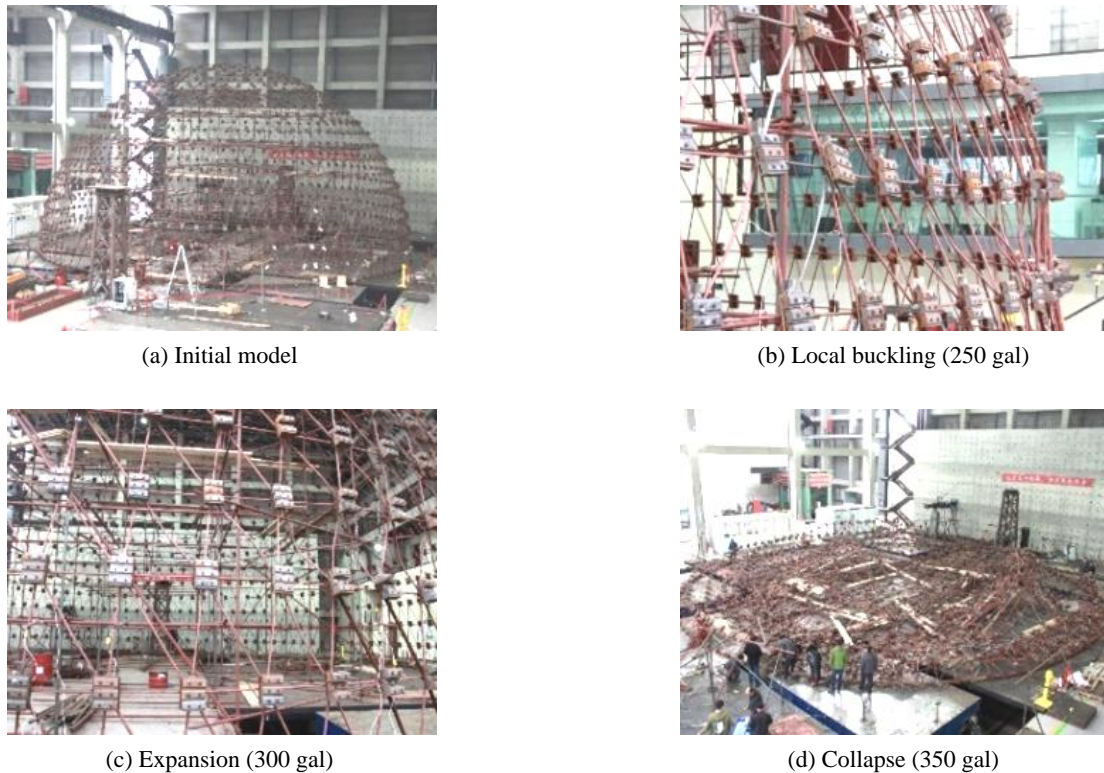


Fig. 13 Experiment of model 2

As the PGA reached 200 gal, the model vibrated with obvious amplitude, but no local instability or buckling elements were observed in this stage. When the PGA rose to 250 gal, only the predetermined weak zones deformed suddenly (Fig. 13 (b)). As the PGA increased to 300 gal, the depressed areas presented notable deflection together with expansion to the surroundings (Fig. 13(c)) while the remaining components showed no obvious deformation. The dome collapsed to the ground immediately when the PGA reached 350 gal (Fig. 13(d)). Probably, the instability mode and collapse mode are connected in this case. The weak zones where buckling deformation mainly occurred failed abruptly when subjected to earthquake, triggering a sudden collapse.

The PGA- Δ curve of the initial model (Fig. 12) shows that when the PGA increases to 200 gal, the dome deforms dramatically with a small increment of PGA, presenting a sudden collapse without any warning.

4.3.2.2 Seismic performance of optimum structure

Seismic analysis is conducted on the optimum model 2, as listed in Table 1. The earthquake wave, elastic modulus and the yield strength in the simulation are the same as the initial model.

No obvious deformation of the optimum dome occurs until the PGA reaches 450 gal. Within this stage, the dome vibrates gently and no elements buckle. When the PGA increases to 550 gal, certain diagonal members of the second ring and latitudinal members of the third ring above table C begin to bend. As the PGA reaches 650 gal, the deformation above table C expands, and elements above table A begin to bend as well. The dome collapses from the

area above table C when the PGA increases to 700 gal. The PGA- Δ curves in Fig. 12 demonstrate that the collapse PGA for the optimum dome is 700 gal, and the critical value for the initial model is 350 gal. The collapse PGA of the optimized dome is elevated by a factor of 2. It can also be concluded that the PGA- Δ curve of the optimum dome tends to be smooth as PGA increases, giving clear warnings prior to collapse.

5. Conclusions

The instability mechanism of domes is revealed from a brand new perspective, and an optimization model against instability is formulated. Optimization is performed on two large-scale real-life models. Stability and seismic performance of the optimum domes are investigated and carefully compared.

- External factors are incorporated in the structural vulnerability theory with the introduction of the geometric stiffness matrix. The relative rate of the joint well-formedness is defined as a variation indicator of joint stiffness. Hence, the classical theory is extended to reveal the instability mechanism: the joints with low r_j suffer extreme stiffness deterioration when subjected to load and tend to lose stability. The minimum value of r_j reflects the stability degradation of the entire structure, and the lower value for the dome, the less stability capacity it has.
- Optimization against instability aimed at maximizing

$r_{r,\min}$ with discrete variables is formulated. The design requirements and steel consumption are implemented as constraints in the optimization. The optimization of two real-life large-scale domes proves that the proposed method can effectively enhance the buckling capacity. Despite the differences of the two initial domes, two optimized domes are similar. When the optimization reaches the optimum result, all parameters converge and remain stable. All these prove the robustness, harmony and self-consistency of the method.

- Seismic performances of the optimum domes are checked. The supplemental simulation demonstrates that the optimal domes have better seismic performances than the initial models. The collapse PGA of each optimum model is increased by a factor of 2. In contrast with the initial models, the optimum models present a better collapse mode with large deformation and give clear warning under the same seismic input. Moreover, there seems to be a correlation between buckling mode and collapse mode. Further researches remain to be done.

Acknowledgments

This work was supported in part by the National Key R&D Program of China [Grant No. 2017YFC1500702], and in part by the Postgraduate Research & Practice Innovation Program of Jiangsu Province [Grant No. KYCX17_0123].

References

- Agarwal, J., Blockley, D. and Woodman, N. (2001), "Vulnerability of 3-dimensional trusses", *Struct. Safety*, **23**(3), 203-220.
- Artar, M. (2016), "A comparative study on optimum design of multi-element truss structures", *Steel Compos. Struct., Int. J.*, **22**(3), 521-535.
- Borri, C. and Spinelli, P. (1988), "Buckling and post-buckling behavior of single layer reticulated shells affected by random imperfections", *Comput. Struct.*, **30**(4), 937-943.
- Cai, J., Zhou, Y., Xu, Y. and Feng, J. (2013), "Non-linear stability analysis of a hybrid barrel vault roof", *Steel Compos. Struct., Int. J.*, **14**(6), 571-586.
- Cai, J., Zhang, Q., Jiang, Y., Xu, Y., Feng, J. and Deng, X. (2017a), "Nonlinear stability analysis of a radially retractable hybrid grid shell in the closed position", *Steel Compos. Struct., Int. J.*, **24**(3), 287-296.
- Cai, J., Liu, Y., Feng, J. and Tu, Y. (2017b), "Nonlinear stability analysis of a radially retractable suspen-dome", *Adv. Steel Constr.*, **13**(2), 117-131.
- Crisfield, M.A. (1983), "An arc-length method including line searches and accelerations", *Int. J. Numer. Methods Eng.*, **19**(9), 1269-1289.
- Dubina, D. (1992), "Computation models and numerical solution procedures for nonlinear analysis of single layer lattice shells", *Int. J. Space Struct.*, **7**(4), 321-333.
- England, J., Agarwal, J. and Blockley, D. (2008), "The vulnerability of structures to unforeseen events", *Comput. Struct.*, **86**(10), 1042-1051.
- GB50017-2003 (2003), Code for design of steel structures, Ministry of housing and urban-rural development of the People's Republic of China; Beijing, China.
- GB/T17395-2008 (2008), Dimensions, shape, mass and tolerances of seamless steel tubes, Standardization administration of the People's Republic of China; Beijing, China.
- Gen, M. and Cheng, R. (1996), "A survey of penalty techniques in genetic algorithms", *Proceedings of 1996 IEEE International Conference on Evolutionary Computation*, IEEE, Nagoya, Japan, May.
- Ghasemi, A.R. and Hajmohammad, M.H. (2015), "Minimum-weight design of stiffened shell under hydrostatic pressure by genetic algorithm", *Steel Compos. Struct., Int. J.*, **19**(1), 75-92.
- Gholizadeh, S. and Barati, H. (2014), "Topology optimization of nonlinear single layer domes by a new metaheuristic", *Steel Compos. Struct., Int. J.*, **16**(6), 681-701.
- Gioncu, V. (1995), "Buckling of reticulated shells: state-of-the-art", *Int. J. Space Struct.*, **10**(1), 1-46.
- JGJ7-2010 (2010), Technical specification for space frame structures, Ministry of housing and urban-rural development of the People's Republic of China; Beijing, China.
- Kamat, M.P., Khott, N.S., Venkayyat, V.B., Kamat, M.P., Khott, N.S. and Venkayyat, V.B. (1984), "Optimization of shallow trusses against limit point instability", *AIAA J.*, **22**(3), 403-408.
- Kashani, M. and Croll, J. (1994), "Lower bounds for overall buckling of spherical space domes", *J. Eng. Mech.*, **120**(5), 949-970.
- Khot, N.S. (1983), "Nonlinear analysis of optimized structure with constraints on system stability", *AIAA J.*, **21**(8), 1181-1186.
- Kloppel, K. and Schardt, R. (1962), "Zur berechnung von netzkuppeln", *Der Stahlbau*, **31**(5), 129-136. [In German]
- Levy, R. (1994a), "Optimal design of trusses for overall stability", *Comput. Struct.*, **53**(5), 1133-1138.
- Levy, R. (1994b), "Optimization for buckling with exact geometries", *Comput. Struct.*, **53**(5), 1139-1144.
- Li, P. and Wu, M. (2017), "Stabilities of cable-stiffened cylindrical single-layer latticed shells", *Steel Compos. Struct., Int. J.*, **24**(5), 591-602.
- Liew, J.R., Punniyakotty, N.M. and Shanmugam, N.E. (1997), "Advanced analysis and design of spatial structures", *J. Constr. Steel Res.*, **42**(1), 21-48.
- Liu, W. and Ye, J. (2014), "Collapse optimization for domes under earthquake using a genetic simulated annealing algorithm", *J. Constr. Steel Res.*, **97**, 59-68.
- Lu, M. and Ye, J. (2017), "Guided genetic algorithm for dome optimization against instability with discrete variables", *J. Constr. Steel Res.*, **139**, 149-156.
- Lu, Z., Yu, Y., Woodman, N.J. and Blockley, D.I. (1999), "A theory of structural vulnerability", *Struct. Engineer*, **77**(18), 17-24.
- Nanghai, Z. and Jihong, Y. (2014), "Structural vulnerability of a single-layer dome based on its form", *J. Eng. Mech.*, **140**(1), 112-127.
- Papadrakakis, M. (1983), "Inelastic post-buckling analysis of trusses", *J. Struct. Eng.*, **109**(9), 2129-2147.
- Pyrz, M. (1990), "Discrete optimization of geometrically nonlinear truss structures under stability constraints", *Struct. Optimiz.*, **2**(2), 125-131.
- Ragon, S.A., Gurdal, Z. and Watson, L.T. (2002), "A comparison of three algorithms for tracing nonlinear equilibrium paths of structural systems", *Int. J. Solids Struct.*, **39**(3), 689-698.
- Riks, E. (1979), "An incremental approach to the solution of snapping and buckling problems", *Int. J. Solids Struct.*, **15**(7), 529-551.
- Riks, E. (1984), "Some computational aspects of the stability analysis of nonlinear structures", *Comput. Methods Appl. Mech. Eng.*, **47**(3), 219-259.
- Saka, M.P. and Geem, Z.W. (2013), "Mathematical and metaheuristic applications in design optimization of steel frame

- structures: an extensive review”, *Math. Problems Eng.*
DOI: 10.1155/2013/271031
- Saka, M.P. and Ulker, M. (1992), “Optimum design of geometrically nonlinear space trusses”, *Comput. Struct.*, **42**(3), 289-299.
- Shen, S.Z. and Chen, X. (1999), *Stability of Reticulated Shells*, Science Press, Beijing, China. [In Chinese]
- Starossek, U. (2007), “Typology of progressive collapse”, *Eng. Struct.*, **29**(9), 2302-2307.
- Stolpe, M. (2016), “Truss optimization with discrete design variables: A critical review”, *Struct. Multidiscipl. Optimiz.*, **53**(2), 349-374.
- Talasilaoglu, T. (2012), “Multiobjective size and topology optimization of dome structures”, *Struct. Eng. Mech., Int. J.*, **43**(6), 795-821.
- Talasilaoglu, T. (2013), “Global stability-based design optimization of truss structures using multiple objectives”, *Sadhana*, **38**(1), 37-68.
- Wang, X., Feng, R.Q., Yan, G.R., Liu, F.C. and Xu, W.J. (2016), “Effect of joint stiffness on the stability of cable-braced grid shells”, *Int. J. Steel Struct.*, **16**(4), 1123-1133.
- Wu, X. (1991), “Vulnerability analysis of structural systems”, Ph.D. Dissertation; University of Bristol, UK.
- Wu, X., Blockley, D.I. and Woodman, N.J. (1993), “Vulnerability of structural systems part 1: rings and clusters”, *Civil Eng. Syst.*, **10**(4), 301-317.
- Xu, L. and Ye, J. (2017), “DEM algorithm for progressive collapse simulation of single-layer reticulated domes under multi-support excitation”, *J. Earthq. Eng.*, 1-28.
DOI:10.1080/13632469.2017.1309606
- Ye, J., Liu, W. and Pan, R. (2011), “Research on failure scenarios of domes based on form vulnerability”, *Sci. China Technol. Sci.*, **54**(11), 2834-2853.